Journal of The Electrochemical Society, **148** (10) F195-F199 (2001)
0013-4651/2001/148(10)/F195/5/$7.00 © The Electrochemical Society, Inc.

X-Ray Reflectivity and FTIR Measurements of N_2 Plasma Effects on the Density Profile of Hydrogen Silsesquioxane Thin Films

H. J. Lee,[a] E. K. Lin,[a] W. L. Wu,[a] B. M. Fanconi,[a] J. K. Lan,[b,c] Y. L. Cheng,[b,c] H. C. Liou,[d] Y. L. Wang,[b] M. S. Feng,[c] and C. G. Chao[c]

[a]*National Institute of Standards and Technology, Polymers Division, Gaithersburg, Maryland 20899, USA*
[b]*Taiwan Semiconductor Manufacturing Company, Hsin-Chu, Taiwan*
[c]*National Chiao-Tung University, Hsin-Chu, Taiwan*
[d]*Dow Corning, Semiconductor Fabrication Materials KCI, USA*

The density depth profile and chemical bond structure of hydrogen silsesquioxane (HSQ) thin films treated with an N_2 plasma with varying power and exposure time were measured using specular X-ray reflectivity (SXR) and Fourier transform infrared (FTIR) spectroscopy. The SXR data indicated that the density profile of an untreated HSQ film is not uniform. At least four layers with different electron densities were required to fit the SXR data. For HSQ films treated with either increasing plasma power or plasma exposure time, the film roughness increased and a densified layer was observed at the film/air interface. The thickness of the densified layer increased with both plasma power and plasma exposure time. In the FTIR spectra of the plasma-treated films, the intensities of the Si-O peaks due to the network structure and the Si-OH peak due to water absorption increased and the intensities of the Si-H peaks decreased. The FTIR data show that the plasma converts the HSQ structure into a SiO_2-like structure and are consistent with the densification observed in the SXR measurements. In general, the HSQ film is more sensitive to increasing plasma power than to increasing plasma exposure time.
© 2001 The Electrochemical Society. [DOI: 10.1149/1.1396338] All rights reserved.

Manuscript received October 16, 2000. Available electronically August 21, 2001.

As device dimensions in integrated circuits (IC) continue to shrink below 0.25 μm, interconnect delay (RC delay) becomes a limiting factor in improving device performance. There are two ways to reduce RC delay, because the delay is a simple product of the resistance between the metal line interconnects and the capacitance of the interlayer dielectric (ILD) material. One solution is to lower the resistance of the metal line and the other is to lower the dielectric constant of the ILD material. Today, copper has replaced aluminum as the metal line material and has received much attention because of its low resistivity and high electromigration resistance. Also, many new ILD materials with low dielectric constants (low-*k*) have been developed to replace the current dielectric, silicon dioxide. One of the most promising low-*k* materials is the commercially available siloxane-based hydrogen silsesquioxane (HSQ) resin. HSQ is already used in IC production because of its excellent planarization, gap fill capabilities, and usefulness in nonetch back processes. However, the combination of both copper lines and low-*k* dielectrics as interconnect materials still has several important technical problems such as reducing copper diffusion, decreasing the leakage current, suppressing water uptake, and avoiding damage during patterning in IC applications. Many researchers are developing new processes with HSQ to address these problems.[1-6]

Many of these problems can be addressed through processes that increase the surface density of an HSQ film. Although this solves some problems, a densified surface layer also increases the effective dielectric constant of film. To balance these two effects, the semiconductor industry would like to precisely control the thickness of the densified dielectric layer. To reach this goal, it is also essential to develop an accurate analytic technique to measure the thickness of the densified dielectric layer. However, few experimental techniques are able to perform high resolution measurements of the density profile of dielectric thin films that are several thousand angstroms thick.

In this work, we demonstrate the use of specular X-ray reflectivity (SXR) as a powerful technique to measure the depth profile of N_2 plasma treated HSQ films. SXR is a nondestructive measurement that allows current instruments to be capable of angstrom resolution for films up to 1.2 μm thick. The influence of the N_2 plasma treatments on the chemical bonding structures of the HSQ films is also investigated using Fourier transform infrared (FTIR) spectroscopy. Data from the FTIR spectra are then correlated with the SXR results to provide both structural and spectroscopic data about plasma-treated HSQ thin films.

Experimental

Films were prepared by spin-coating HSQ resin onto 200 mm silicon wafers, then baked for 1 min sequentially on separate hot plates set at 150, 200, and 350°C. The films were then cured in a furnace at 400°C for 1 h under a N_2 atmosphere. Samples were prepared with two different thicknesses, 300 nm for an HSQ film without plasma treatment, and 400 nm for films undergoing plasma treatments. Several different N_2 plasma post-treatments were applied to the cured HSQ films. In one series of treatments, the samples were placed in the plasma for 60 s while the plasma power was varied from 200 to 600 W. Second, the plasma power was maintained at 400 W while the plasma exposure time was varied from 50 to 80 s.

X-ray reflectivity measurements were performed using a modified high resolution X-ray diffractometer with a tube source using Cu Kα radiation with a wavelength, λ, of 1.54 Å. The incident beam was conditioned with a four-bounce germanium (220) monochromator. Before the detector, the beam was further conditioned with a three-bounce germanium (220) channel cut crystal. The goniometer has an active servo feedback system to provide an angular reproducibility of 0.0001°. This instrumental configuration enables the observation of interference fringes from films with thicknesses up to 1.2 μm. The reflected intensity was collected as a function of the grazing incident angle equal to the detector angle. The measured angular range was 0.1 to 0.6° for the films in this study.

When the grazing incidence angle, θ, of the X-ray beam is smaller than the critical angle of the film, θ_c, the X-ray beam is almost completely reflected. The critical angle is directly related to the electron density of the film through the equation: $\theta_c = \lambda(\rho_e r_e/\pi)^{1/2}$, where ρ_e is the electron density and r_e is the classical electron radius, 2.818 fm. The momentum transfer in the film thickness direction (Q_z) is also related to the incident angle and is defined as $Q_z = (4\pi/\lambda)\sin\theta$. The precise measurement of the critical angle is an important factor in the determination of the average electron density of the film.

The SXR data were analyzed by fitting model electron density depth profiles to the experimental data using a least squares fitting

Downloaded on 2014-04-27 to IP 140.113.38.11 address. Redistribution subject to ECS terms of use (see ecsdl.org/site/terms_use) unless CC License in place (see abstract).

routine based upon the algorithm of Parratt.[7,8] The theoretical basis of the deconvolution of the SXR data is described in detail elsewhere.[9] The depth profile of the electron density of the film is modeled as a series of layers each characterized by an electron density, thickness, and interfacial width or roughness. The primary parameter used to describe the model profile is Q_c^2, the elastic coherent scattering per unit volume, and is directly proportional to the electron density. Given an elemental composition, Q_c^2 values are easily converted into a mass density. The reflectivity is calculated for a model profile and compared with the experimental data. The model electron density profile is then numerically adjusted until the calculated reflectivity agrees well with the data.

Infrared absorption spectra with wavenumbers ranging from 400 to 4000 cm^{-1} were recorded with a spectrometer with 4 cm^{-1} spectral resolution. The data from each sample were averaged over 100 scans to increase the signal to noise ratio. The final sample spectra were obtained after subtracting the peaks due to the silicon substrate.

Results and Discussion

Figure 1 shows the SXR curve for the untreated cured HSQ film presented as the logarithm of the ratio of the reflected beam intensity (I) to the incident beam intensity (I_o) *vs.* Q_z. Two critical angles arising from the dielectric material and the silicon substrate are observed in the reflectivity data. The first critical angle (due to the dielectric thin film) is at $Q_z = (0.0255 \pm 0.0005)$ $Å^{-1}$ and the second angle (due to the silicon substrate) is at $Q_z = (0.0310 \pm 0.0006)$ $Å^{-1}$.[7,e] Constructive and destructive interference between radiation reflected from the air/film interface and the film/silicon interface results in oscillations in the SXR curve. The overall thickness of the film can be determined from the spacing of the interference fringes in the SXR data because the periodicity of the oscillations is proportional to the dielectric film thickness [thickness = 2π/(fringe spacing)].[7] However, at low Q_z values near the critical angle of silicon, the linear relationship between film thickness and the periodicity of the interference fringes is affected by multiple scattering. At larger Q_z values when the reflectivity is less than 10^{-2}, multiple scattering contributions to the reflectivity signal are less than 1% of the reflected intensity. In this work, the film thickness of HSQ was determined from the spacing of the fringes in the Q_z region ranging from 0.053 to 0.092 $Å^{-1}$. The thickness of the film in Fig. 1 is (316 ± 1) nm.

The best fit to the experimental data of untreated HSQ film is also shown in Fig. 1. This HSQ film requires at least four distinct layers to adequately fit the data. Figure 2 shows the electron density profile corresponding to the best fit to the HSQ reflectivity data. This profile includes a dense top layer about 5 nm thick as well as a layer, about 51 nm thick, that is slightly denser than pure HSQ. The electron density of the top layer is approximately 92% of the density of quartz, suggesting that this layer was transformed into a structure similar to silicon dioxide. The density of the second layer is higher than the third layer (pure HSQ), by a fraction, approximately 3%. The densification in the second layer is likely due to the loss of Si-H bonds and some film oxidation during the bake and cure processes. Interestingly, there is also a less dense layer, approximately 6 nm thick, near the silicon substrate with a density that is 91% of the bulk HSQ layer.

Figure 3 shows the SXR data from a series of HSQ films after plasma treatment for 60 s with plasma powers varying from 200 to 600 W. Figure 4 shows the SXR data from a series of HSQ films after plasma treatment at a plasma power of 400 W for times varying from 50 to 80 s. There are several general characteristics that appear in the SXR data of each of the plasma treated films. Relative to the untreated HSQ film, the amplitude of the oscillations in the SXR data decrease and the specular reflectivity drops more quickly be-

[e] All data in the text and in the figures are presented with the standard uncertainty (±) associated with the measurement.

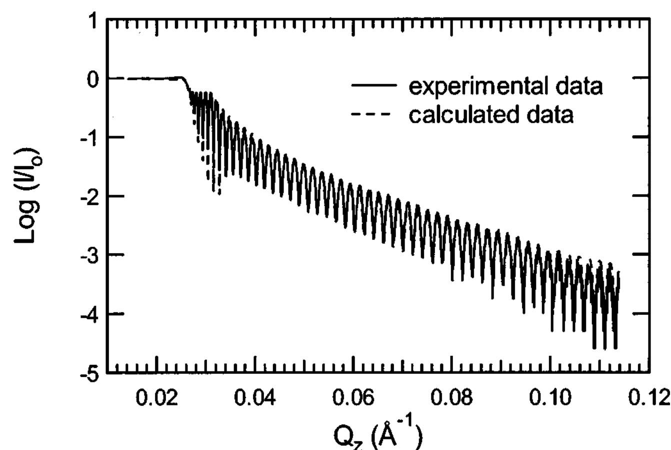

Figure 1. SXR curve of HSQ film without plasma treatment as presented as the logarithm of the ratio of the reflected beam intensity (I) to the incident beam intensity (I_o) *vs.* the magnitude of the momentum transfer in the film thickness direction (Q_z). The solid and dotted curves represent the experimental and calculated data, respectively.

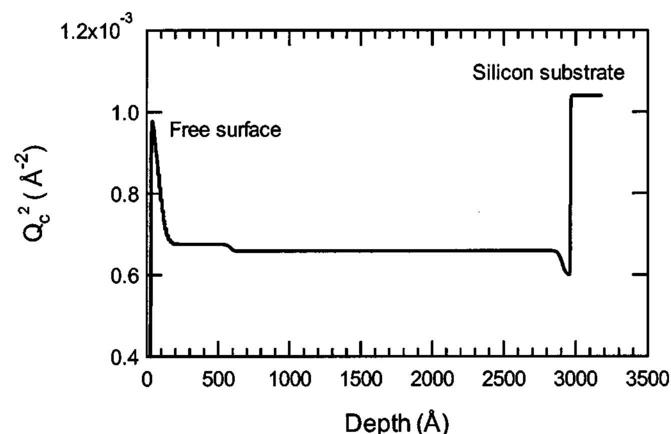

Figure 2. Calculated electron density depth profile of the film in Fig. 1. The free surface is located at the far left of the horizontal axis and the silicon substrate is located at the far right of the abscissa.

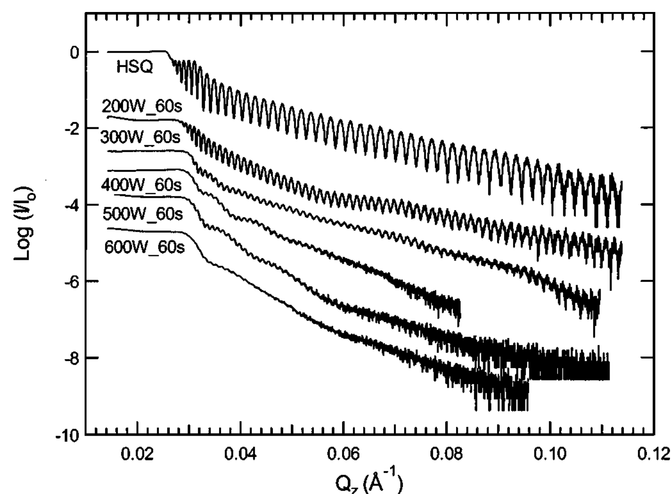

Figure 3. SXR curves of plasma-treated HSQ films treated with different plasma powers for 60 s presented as the logarithm of the ratio of the reflected beam intensity (I) to the incident beam intensity (I_o) *vs.* the magnitude of the momentum transfer in the film thickness direction (Q_z).

Downloaded on 2014-04-27 to IP 140.113.38.11 address. Redistribution subject to ECS terms of use (see ecsdl.org/site/terms_use) unless CC License in place (see abstract).

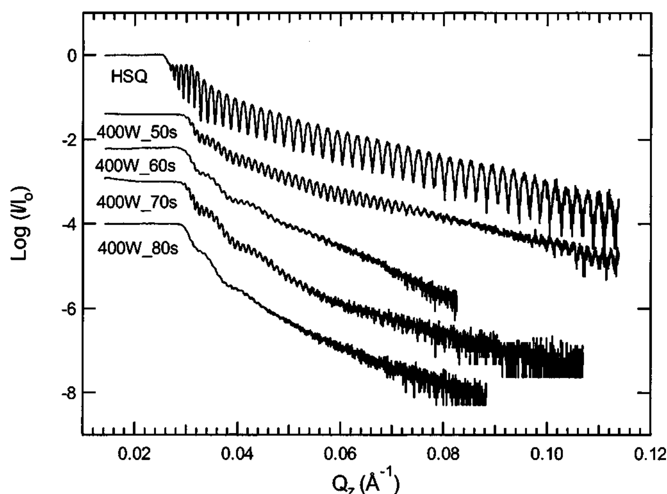

Figure 4. SXR curve of plasma-treated HSQ films with a plasma power of 400 W and different plasma exposure times presented as the logarithm of the ratio of the reflected beam intensity (I) to the incident beam intensity (I_o) *vs.* magnitude of the momentum transfer in the film thickness direction (Q_z).

yond critical angle indicating that the film roughness is increasing. When the roughness of the film increases, the specular reflectance at angles beyond the critical angle decreases faster than those values calculated for an ideal smooth interface using the Fresnel equations.[9-11] Additionally, when the plasma power and plasma exposure time increase, a longer wavelength oscillation appears in each SXR curve and the critical angle of the HSQ film moves to higher values indicating that a thinner denser layer has formed within the film. Fits to the SXR data are shown in Fig. 5 and 6. Up to seven distinct thin film layers as well as the silicon substrate layer were required to adequately model the SXR data from the plasma-treated samples.

For comparison, we compare the plasma treated films with conventional silicon dioxide materials. The Q_c^2 values or electron densities of fully densified quartz and plasma enhanced chemical vapor deposition (PECVD) tetraethoxysilane (TEOS) dioxide are reported to be 1.14×10^{-3} and 0.887×10^{-3} Å^{-2}, respectively.[12] In this work, we define a fully densified film as a film having a density larger than the density of PECVD TEOS oxide and a densified layer as a layer with a larger density than that of bulk HSQ or the cured HSQ. The HSQ film treated with N_2 plasma at 200 W for 60 s shows an almost fully densified layer approximately 14 nm thick. In Fig. 7,

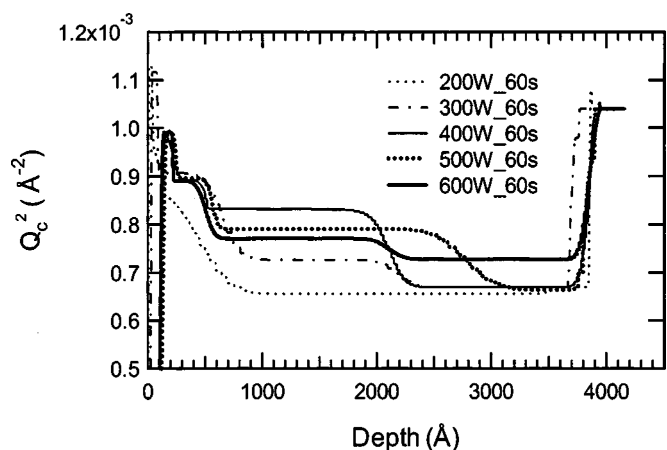

Figure 5. Electron density depth profiles of HSQ films treated with different plasma power ranging from 200 to 600 W for 60 s.

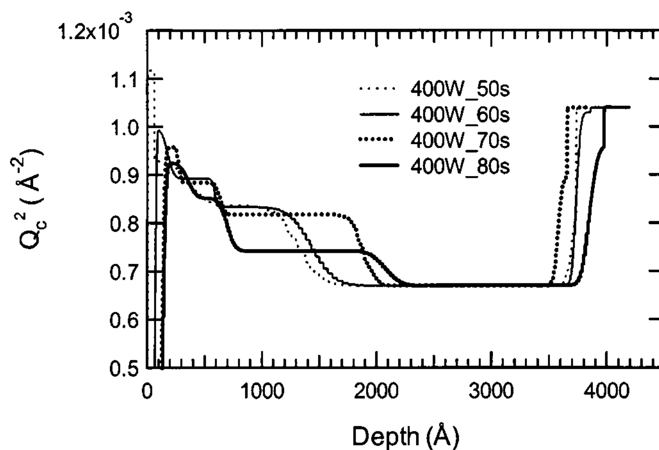

Figure 6. Electron density depth profiles of HSQ films treated at 400 W of power for different plasma exposure time ranging 50 to 80 s.

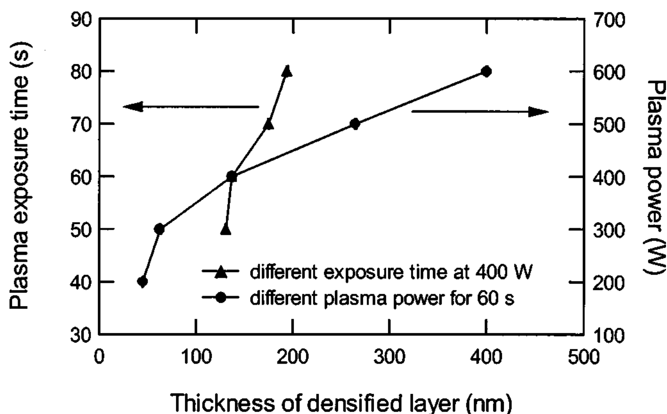

Figure 7. The thickness of the densified layers of HSQ films with different plasma treatment conditions. Errors are smaller than the size of the symbols.

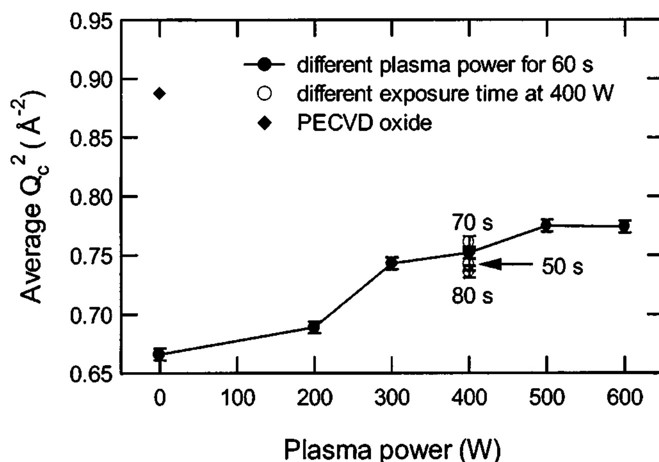

Figure 8. Average Q_c^2 of HSQ films with different plasma treatment conditions. For reference, the average Q_c^2 of PECVD TEOS oxide and the as-cured HSQ films are also shown.

Downloaded on 2014-04-27 to IP 140.113.38.11 address. Redistribution subject to ECS terms of use (see ecsdl.org/site/terms_use) unless CC License in place (see abstract).

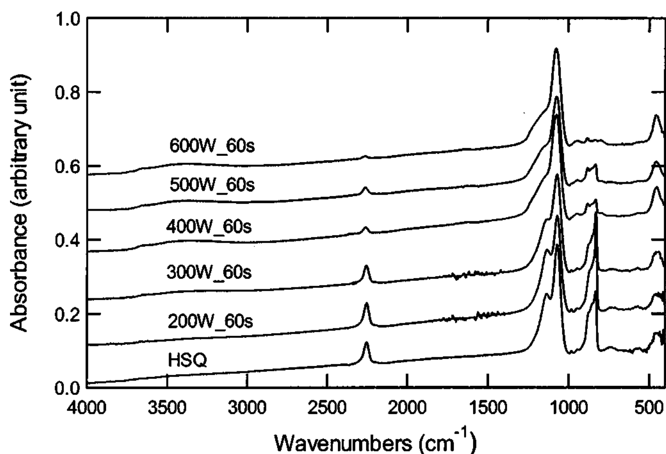

Figure 9. FTIR spectra of plasma-treated HSQ films with different plasma powers presented as relative intensity of absorbance *vs.* wavenumbers.

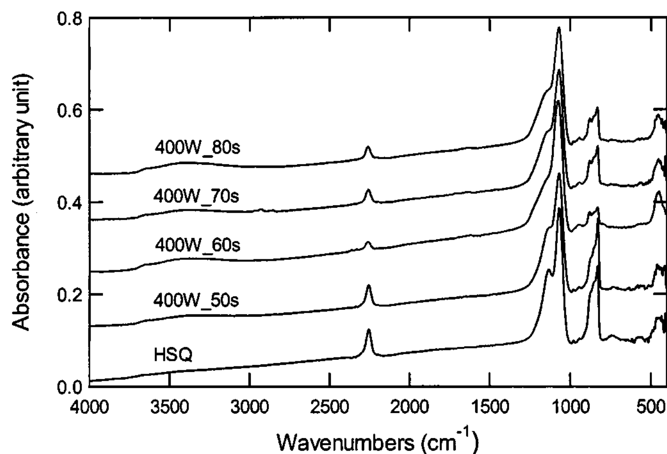

Figure 10. FTIR spectra of plasma-treated HSQ films with different plasma exposure time presented as relative intensity of absorbance *vs.* wavenumbers.

we plot the thickness of the densified layer as a function of different plasma treatment conditions. The thickness of the densified layer formed by the plasma treatment generally increases with plasma power and plasma exposure time. More specifically, when the exposure time was fixed at 60 s, the thicknesses of the densified layers were approximately 45, 63, 137, and 265 nm, for plasma powers of 200, 300, 400, and 500 W, respectively. When the plasma power was 600 W and the exposure time was 60 s, the entire HSQ film (approximately 400 nm thick) was densified by the plasma. When the plasma power was fixed at 400 W and the plasma exposure times were 50, 70, and 80 s, the thicknesses of the densified HSQ films were approximately 131, 175, and 194 nm, respectively. Figure 7 also shows that the effect of plasma power on the thickness of the densified layer in the HSQ film is much larger than the effect of the plasma exposure time.

In Fig. 8, we plot the average densities of the plasma treated HSQ films as a function of different plasma conditions. The average densities of the films are calculated using the Q_c^2 and thickness of each layer used in the model profile through the summation of (Q_c^{2}* thickness/total film thickness). The density of a PECVD oxide is also shown in Fig. 8 to provide a reference value to compare the relative degree of densification within each film. The average density of an HSQ film treated at 200 W for 60 s increases only by a fraction, 3% above the untreated HSQ film. The HSQ films are densified much more for plasma powers greater than 300 W and the percent densification relative to PECVD silicon oxide appears to saturate for plasma powers greater than 500 W. An HSQ film with plasma treatment of 600 W for 60 s is densified to approximately 87% of the density of PECVD oxide. This suggests that a fraction of the initial cage structure remains in the film even though the entire HSQ film treated at 600 W for 60 s is affected by the plasma.

FTIR spectra are taken to verify the postulated chemical structure changes of the densified HSQ films. The FTIR spectra of the HSQ films with and without plasma treatment are shown in Fig. 9 and 10. The important modes in the FTIR spectra are the $\nu(O_3Si\text{-}H)$ stretching mode near 2250-2260 cm^{-1} and the two ν_{as}(Si-O-Si) asymmetric stretching modes near 1068-1078 cm^{-1} and 1132-1136 cm^{-1}. One ν_{as}(Si-O-Si) peak has a higher wavenumber and corresponds to the stretching of larger angle (Si-)O-Si bonds within the HSQ cage structure. The other ν_{as}(Si-O-Si) peak has a smaller wavenumber and represents the stretching of smaller angle (Si-)O-Si bonds within the cured network structure.[13,14] As the plasma power and plasma exposure time increases, the intensity of the 1068 cm^{-1} band grows more pronounced relative to the 1135 cm^{-1} band because the plasma cleaves the silsesquioxane cages in the HSQ films and transforms the HSQ film into a SiO_2-like structure. Also, increasing the plasma power and plasma exposure time causes the intensity of the peaks from the smaller angle (Si-)O-Si band to shift to a higher frequency because of the back-bonding coordination of oxygen atoms. Additionally, the plasma-treated films show that more Si-H bonds in the HSQ film are converted into Si-O bonds leaving more oxygen atoms around a Si atom. These electronegative oxygen atoms effectively attract electrons away from neighboring Si-O bonds resulting in an increased Si-O bond strength or bond energy.[15,16]

The intensities of the three bands from the (H-)Si-O bending mode at 830, 856, and 876 cm^{-1} and the sharp band from the (O_3-)Si-H stretching mode at 2254 cm^{-1} decrease due to the

Table I. The characteristic peak position (cm^{-1}) of different bonds from HSQ films after various plasma treatment conditions. Standard uncertainty associated with the measurement of all data is ±0.5 cm^{-1}.

Samples	$\nu_{as}{}^{b}$(Si-O-Si)	$\nu(O_3Si\text{-}H)$	H_2SiO	d^b(HSi-O)
HSQ w/o plasma	1068, 1135	2254	2195, 982, 945	876, 856, 830
HSQ/200 W_60 s	1068, 1132	2254	2195, 982, 948	828
HSQ/300 W_60 s	1069, 1135	2255	2198, 982, 947	829
HSQ/400 W_60 s	1075, sh*[a]	2260	983, 947	830
HSQ/500 W_60 s	1072, sh*	2262	2203, 983, 946	831
HSQ/600 W_60 s	1078, sh*	2263	-	832
HSQ/400 W_50 s	1069, 1136	2255	2195, 981, 946	828
HSQ/400 W_70 s	1070, sh*	2257	2203, 982, 944	830
HSQ/400 W_80 s	1070, sh*	2259	2204, 983, 945	831

[a] sh* represents shoulder without isolated peak.
[b] ν and d represent the stretching and bending modes, respectively.

Downloaded on 2014-04-27 to IP 140.113.38.11 address. Redistribution subject to ECS terms of use (see ecsdl.org/site/terms_use) unless CC License in place (see abstract).

plasma-induced cleavage of the cage structure and of the Si-H bonds in the HSQ films. The cleavage of cages is more strongly influenced by increasing the plasma power than increasing the plasma exposure time. After plasma treatment at 600 W for 60 s, the (H-)Si-O bending and (O_3-)Si-H stretching peaks of the initial HSQ film almost disappear, indicating that the entire HSQ film is affected and transformed into a SiO_2-like structure by the N_2 plasma. As the Si-H peak intensity diminishes, the (Si-)O-Si bending peak below 500 cm^{-1} clearly increases. The intensities of the three peaks due to the H_2SiO moiety at 945, 982, and 2195 cm^{-1} decrease with increasing plasma power and plasma exposure time. Previous researchers have reported that N_2 plasma treatments cause the Si-H bonds in HSQ to break leaving many dangling bonds in the film.[4] Some of these dangling bonds immediately absorb water after exposure to ambient air. When the plasma power is larger than 300 W, adsorbed water appears in the FTIR spectra from the broad peak centered at 3400 cm^{-1} and the relatively sharp Si-OH peak at 3654 cm^{-1}. The other absorption band assignments in the FTIR spectra of the plasma treated films are listed in Table I.

Conclusions

We have demonstrated that high resolution SXR measurements provide a unique and promising method to obtain detailed information about the density profile and average density of plasma treated low-*k* dielectric thin films. Using this technique, process and materials engineers will be able to better evaluate process design methods to optimize the film density for future IC applications using low-*k* dielectric materials. We determined that the best-fit model profile for the SXR data from an as-cured HSQ film required at least four distinct layers with different electron densities. Plasma-treated HSQ films required up to seven separate layers to adequately fit the data. A densified HSQ layer with a density approaching a SiO_2-like density was observed for all films studied here. Both the thickness of the densified layer and the film roughness at the film/air interface increased with increasing plasma power and plasma exposure time. The densification of and the change in bond environment in the HSQ films with and without plasma treatment were characterized using FTIR measurements. The FTIR spectra suggest that the HSQ cage structure is transformed into a SiO_2-like one by the plasma and are consistent with the densification observed by SXR. In the future, we plan to extend these measurements to porous low-*k* dielectric thin films. Plasma treatments for porous low-*k* dielectric materials are of interest because porous films have much weaker physical properties requiring the development of new processes to increase the film density without lowering the dielectric constant.

The National Institute of Standards and Technology assisted in meeting the publication costs of this article.

References

1. P. T. Liu, T. C. Chang, Y. L. Yang, Y. F. Cheng, F. Y. Shih, J. K. Lee, E. Tsai, and S. M. Sze, *Jpn. J. Appl. Phys., Part 1,* **38**, 6247 (1999).
2. K. M. Chang, I. C. Deng, S. J. Yeh, and Y. P. Tsai, *Electrochem. Solid-State Lett.,* **2**, 634 (1999).
3. S. W. Chung, J. H. Shin, N. H. Park, and J. W. Park, *Jpn. J. Appl. Phys., Part 1,* **38**, 5214 (1999).
4. P. T. Liu, T. C. Chang, S. M. Sze, F. M. Pan, Y. J. Mei, W. F. Wu, M. S. Tsai, B. T. Dat, C. Y. Chang, F. Y. Shih, and H. D. Huang, *Thin Solid Films,* **332**, 345 (1998).
5. T. C. Chang, M. F. Chou, Y. J. Mei, J. S. Tsang, F. M. Pan, W. F. Wu, M. S. Tsai, C. Y. Chang, F. Y. Shih, and H. D. Huang, *Thin Solid Films,* **332**, 351 (1998).
6. P. T. Liu, T. C. Chang, Y. L. Yang, Y. F. Cheng, J. K. Lee, F. Y. Shih, E. Tsai, G. Chen, and S. M. Sze, *J. Electrochem. Soc.,* **147**, 1186 (2000).
7. W. L. Wu, W. E. Wallace, E. K. Lin, G. W. Lynn, C. J. Glinka, E. T. Ryan, and H. M. Ho, *J. Appl. Phys.,* **87**, 1193 (2000).
8. W. L. Wu and H. C. Liou, *Thin Solid Films,* **312**, 73 (1998).
9. L. G. Parratt, *Phys. Rev.,* **95**, 359 (1954).
10. G. S. Lodha, K. Yamashita, H. Kunieda, Y. Tawara, J. Yu, Y. Namba, and J. M. Bennett, *Appl. Opt.,* **37**, 5239 (1998).
11. S. Santucci, A. V. L. Cecilia, A. R. Phani, R. A. Alfonsetti, G. Moccia, and M. D. Biase, *Appl. Phys. Lett.,* **76**, 52 (2000).
12. W. E. Wallace, W. L. Wu, and R. A. Carpio, *Thin Solid Films,* **280**, 37 (1996).
13. M. J. Loboda, C. M. Grove, and R. F. Schneider, *J. Electrochem. Soc.,* **145**, 2861 (1998).
14. M. G. Albrecht and C. Blanchette, *J. Electrochem. Soc.,* **145**, 4019 (1998).
15. P. A. Agaskar, V. W. Day, and W. G. Klemperer, *J. Am. Chem. Soc.,* **109**, 5554 (1987).
16. G. Lucovski, J. Yang, S. S. Chao, J. E. Tyler, and W. Czubatyj, *Phys. Rev. B,* **28**, 3225 (1983).

Downloaded on 2014-04-27 to IP 140.113.38.11 address. Redistribution subject to ECS terms of use (see ecsdl.org/site/terms_use) unless CC License in place (see abstract).